Nanoscale

Accepted Manuscript

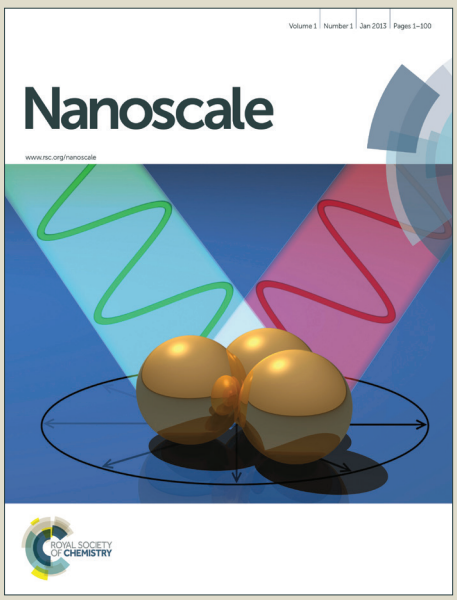

ROYAL SOCIETY OF CHEMISTRY

www.rsc.org/nanoscale

Journal Name

ARTICLE

Practical and High Sensitive C_3N_4-TYR Fluorescent Probe for Convenient Detection of Dopamine

Received 00th January 20xx,
Accepted 00th January 20xx

DOI: 10.1039/x0xx00000x

www.rsc.org/

Hao Li‡, Manman Yang‡, Juan Liu, Yalin Zhang, Yanmei Yang, Hui Huang*, Yang Liu*, Zhenhui Kang*

The C_3N_4-tyrosinase (TYR) hybrid, as a fluorescent probe, is highly accurate, sensitive and simple for the detection of Dopamine (DOPA). Under the optimized conditions, the relative fluorescence intensity of C_3N_4-TYR is proportional to the DOPA concentration in the concentration range from the 1×10^{-3} to 3×10^{-8} mol L^{-1} with correlation coefficient of 0.995. In the present system, the detection limit is achieved to 3×10^{-8} mol L^{-1}. Notably, those quantitative detection results of clinic samples are comparable to those of the high performance liquid chromatography methods. Moreover, the enzyme-encapsulated C_3N_4 sensing arrays on glass slide and test paper were performed, which reveals the sensitive sensing and excellent stability. The results reported here provide a new approach to design multifunctional nanosensor for the detection of bio-molecules.

Introduction

Dopamine (DOPA) is an important neurotransmitter and hormone for people and animals in the catecholamine and phenethylamine families, [1] which is implicated in locomotion, reward and motivation.[2] If the deficiency of DOPA in the brain beyond the normal that will cause in pathogenesis of neurological disorders such as Parkinson's disease, Schizophrenia and Huntington's disease.[3–6] Therefore, this has sparked significant interest for the development of detection methods for DOPA. Various analytical methods such as high performance liquid chromatography (HPLC) and electrochemical techniques have been used for the detection of DOPA.[7] However, these methods need complicated pre-concentration, time-consuming steps, high-cost instruments, and sophisticated equipment, which tremendously limit their wide application. Therefore, an easy, exact and fast method for the detection of DOPA is highly needed.

Compared with conventional analytical techniques, fluorescent biosensor, [8] as a new class of detection method, has caused a great deal of attention for the detection of DOPA due to its high sensitivity, low cost and practicality. As known, the practical fluorescent biological probes should satisfy three points as follows: firstly, the emission spectroscopy of biosensor must match the absorption spectrum of dopaminechrome (products of oxidation by the enzyme). Secondly, the fluorescent sensor material should have the proton (H^+) adsorption and/or electron acceptors ability. Thirdly, the fluorescent sensor material should possess low toxicity and biocompatibility. Recently, the semiconductor based quantum dots (QDs) are regarded as powerful inorganic fluorescent probes.[9] For example, Yuan et al. used the CdTe quantum dots as a fluorescent indicator to detect the DOPA (detection limit: 0.05 μM, detection range: 50-1000 μM).[10] However, the potential toxicity, and poor biocompatibility limit its further practical applications.[11]

C_3N_4 has attracted more attention due to the easy preparation, high quantum yield, non-toxicity, low cost, good biocompatibility and excellent photostability. [11–17] Particularly, the N-contain-structure make it possess strong proton (H^+) adsorption ability, which is helpful for the fluorescent biosensor design towards the high sensitive detection of DOPA. Herein, we report the C_3N_4-tyrosinase (TYR) as a fluorescent probe (C_3N_4-TYR), which exhibits high accuracy, sensitivity, and simple for the detection of DOPA. In the detection system, the DOPA can be oxidized by TYR to form dopaminequinone, which subsequently quickly be oxidized to dopaminechrome in phosphate buffer (PB). The absorption spectrum of dopaminechrome has heavy overlap with the fluorescence spectrum of C_3N_4, which significantly quenches the fluorescence of C_3N_4. Based on the C_3N_4-TYR fluorescent probe, good linear correlations were obtained in the concentration range from 1×10^{-3} to 3×10^{-8} mol·L^{-1} with the detection limit of 3×10^{-8} mol L^{-1} for the detection of DOPA. Notably, the quantitative detection results of clinic samples are comparable to those of the high performance liquid chromatography (HPLC) method. Moreover, the C_3N_4-TYR sensing arrays on glass slide and test paper were successfully

Jiangsu Key Laboratory for Carbon-Based Functional Materials & Devices, Institute of Functional Nano & Soft Materials (FUNSOM), Soochow University, 199 Ren'ai Road, Suzhou, 215123, Jiangsu, PR China. zhkang@suda.edu.cn; yangl@suda.edu.cn; hhuang0618@suda.edu.cn.
‡ These authors contributed equally to this work.
† Electronic supplementary information (ESI) available. See DOI: 10.1039/x0xx00000x

performed, which reveals the sensitive sensing and excellent stability.

Experimental

Chemicals

Urea and melamine were purchased from Sigma-Aldrich. Tyrosinase (TYR, 845 U/mg) and dopamine were purchased from USA Worthington Biochimical Co. Ltd. All other chemicals used in this work were of analytical grade. Except the specific statement, the detection buffer was PB buffer (pH = 6.8, 0.05 mol L^{-1} sodium phosphate). Milli-Qultrapure water (Millipore, $\geqslant$ 18 MΩ cm) was used throughout.

Characterization

Transmission electron micrographs (TEM) were taken on a FEI/Philips Tecnai G2 F20 (200 kV) TWIN TEM. Scanning electron microscopy (SEM) images were obtained using FEI-quanta 200 scanning electron microscope with acceleration voltage of 20 kV and coupled with an energy-dispersive X-ray analysis (EDX) spectrometer. The Fourier transform infrared (FTIR) spectra were obtained with a Bruker Fourier Transform Infrared Spectrometer (Hyperion). Photoluminescence (PL) study was carried out on a Horiba Jobin Yvon (FluoroMax 4) Luminescence Spectrometer, while UV–Vis spectra were obtained with an Perkin Elmer Lambda 750 spectrophotometer. Powder X-ray diffraction (PXRD) data were collected on an X'Pert-ProMPD (Holand) D/max-γ AX-ray diffractometer with Cu K_α radiation in a flat plate geometry. Atomic force microscopy (AFM) measurements were performed on Veeco Multimode V Atomic Force Microscope. The scans were performed in the tapping mode, using a silicon tip. The Brunauer–Emmett–Teller (BET) specific surface areas and pore size distributions were calculated by plotting the adsorption isotherm of N_2 at liquid N_2 temperature (77 K). These measurements were made on Micromeritics ASAP 2050 porosimeter. DOPA detection using high-performance liquid Chromatography (HPLC) was conducted on HP Agilent 1100 Series HPLC.

Synthesis of C_3N_4

The C_3N_4 power was obtained by directly heating the urea in a semi-closed system with one-step heat treatment. 5 g urea was added in a crucible. Then the crucible was directly heated to 550 ℃ at a rate of 5 ℃ min^{-1} and then kept at this temperature for another 3 h in a muffle furnace.[18]

Synthesis of nonporous-C_3N_4 (g- C_3N_4)

The g-C_3N_4 was prepared according to the literature.[19] The nonporous-C_3N_4 power was obtained by directly heating the melamine in a semi-closed system with two-step heat treatment. Typically, 10 g of melamine was put into an crucible with a cover and first heated at a rate of 20 °C min^{-1} to 500 °C ina muffle furnaceand kept at this temperature for 2 h. Then deammonation treatment was conducted at 550 °C for 2 h (at a a rate of 20 °C min^{-1}).

Preparation of C_3N_4-TYR

In a 50 mL glass tube, the obtained C_3N_4 (0.0168 g), 20 ml phosphate buffer (PB, 0.05 mol L^{-1}, pH = 6.8) and enzyme tyrosinase (TYR, 0.04 g) were added. The mixture was stirred at 4 ℃ for 24 h in cold water bath. Then the mixture was centrifuged (10000 rpm, 30 min) and washed with PB solution for several times. At the same time, the wet C_3N_4-TYR powder was lyophilized by the freezedryer. Finally, 0.05 g freeze-drying C_3N_4-TYR powder was added in 5 mL PB solution, the C_3N_4-TYR solution (0.01 g/mL) was prepared.

Analysts Sensing by PL Detection

For all tests and reactions, the experiments were repeated at least three times to ensure the accuracy of the measurement. All of the PL spectra were recorded on a fluorescence spectrophotometer. The emission spectra were recorded under the excitation wavelength of 390 nm. For the study of the quenching effect of dopamine on TYR-encapsulating C_3N_4, 0.2 mL TYR-encapsulating C_3N_4 was mixed with phosphate buffer (3 mL). Then the dopamine solutions with different concentrations were added into the mixture. Finally, the mixture was incubated at 35 ℃ for 40 min for PL measurements.

C_3N_4-TYR Sensing Arrays on Glass Slide

The prepared C_3N_4-TYR (2 μL, 0.01 g/mL) was dropped on glass slides, dried by evaporation, and stored at 5 ℃. For the analysis sensing, dopamine solution (2.5 μL) of various concentrations were dropped on the sensing arrays and left to interact for 5 min. Fluorescence of the sensing array was observed under excitation with 365 nm light of a UV lamp.

C_3N_4-TYR test paper

The filter papers were immersed into the solution of C_3N_4-TYR (0.003 g/mL). Then dopamine of different concentration was dropped on the filter paper and stored for 40 min at 4 ℃. Fluorescence of the test paper was observed under excitation with 365 nm light of a UV lamp.

Adsorption Equilibrium Measurements

In order to study the proton (H^+) adsorption capacity of C_3N_4, the same concentration 0.005 M HCl solution was selected to investigate the adsorption behaviour of C_3N_4. Because of the water solubility of C_3N_4, the adsorption experiments were conducted with a dialysis method. The C_3N_4 solution was dialyzed using a semi-permeable membrane (MWCO 1000) in a 1000 mL beaker, and the dialysate was 0.005 M HCl (600 mL). Notably, the C_3N_4 was treated previously by dialysis method before using, so, C_3N_4 would not dialyze out of semi-permeable membrane. If C_3N_4 has good adsorption behaviour of H^+, H^+ would gradually cross semi-permeable membrane and dialyze into C_3N_4 solution. After stirring on a shaker for predetermined time intervals, the residual concentration of HCl solution was determined by titrating with 0.005 M NaOH solution.

Data Normalization Method

In order to make the data referenceable, all of the PL spectra were normalized. The peak intensity of PL spectra at 440 nm

was selected as a standard. For detecting the dopamine, the normalized intensity was the ratio of I and I_0, where I and I_0 are the PL intensities of the C_3N_4 in the presence and absence of dopamine, respectively. For investigating the effect irradiation time, temperature, ionic strength and pH to the stability of C_3N_4, and studying the influence of temperature, pH values and incubation time on the reaction system, the normalized intensity was obtained by using the maximum intensity of measurement as reference.

The Detailed Analysis of Michaelis-Menten Equation

In order to test the enzyme activity, Michaelis-Menten analysis was performed. The classic Michaelis-Menten mechanism provides a highly satisfactory description of catalytic activities for large ensembles of enzyme molecules. It yields the relationship between the initial velocity (V) and the substrate concentration [S].

$$\mathbf{V} = \frac{[\mathbf{S}]\mathbf{V_{max}}}{[\mathbf{S}] + \mathbf{K_m}}$$

Where, V_{max} is the maximum velocity of the enzymatic reaction and K_m is the Michaelis constant representing the concentration of substrate at half of the maximum velocity.

$$\frac{\mathbf{1}}{\mathbf{V}} = \frac{\mathbf{K_m}}{\mathbf{V_{max}}}\frac{\mathbf{1}}{[\mathbf{s}]} + \frac{\mathbf{1}}{\mathbf{V_{max}}}$$

By plotting 1/V with 1/[S], the ordinate intercept of the obtained graph is equivalent to the inverse of V_{max}; the abscissa intercept of the graph represents $-1/K_m$. Thus, both K_m and V_{max} values can be calculated.

Results and Discussion

As shown in Figure 1A, the typical TEM image indicates that the obtained C_3N_4 has a thick-layered structure. While Scanning Electron Microscope (SEM) image (Figure S1A) further shows the loose and soft agglomerates with a size of several micrometers. The inset in Figure S1A (the energy-dispersive X-ray (EDX) spectrum) indicates the ratio content of C elements and N elements is about 3:4, further confirming the formation of C_3N_4. The XRD pattern of C_3N_4 is shown in the inset of Figure 1A. The strong peak at 27.57° is the characteristic interlayer stacking peak of aromatic systems,[20] which is indexed for graphitic material as the (002) peak and corresponding to the inter-player d-spacing (0.324 nm) of C_3N_4. While the weak peak at 13.14° is due to the interlayer stacking, which is indexed as (100) and corresponding to an interlayer distance of d = 0.675 nm.[19, 21] UV/Vis absorption spectrum (Figure S2, black line) indicates the absorption edge of the obtained C_3N_4 around 460 nm, corresponding to the intrinsic band gap of C_3N_4 (2.7 eV).[22, 23] Figure S2 (red line) shows the FTIR spectrum of C_3N_4. The peak at around 3500 cm^{-1} corresponds to the N-H stretching. Several bonds in the 1200-1650 cm^{-1} region are associated with the typical stretching modes of C-N heterocycles.[24-28] While the bond at 810 cm^{-1} is corresponding to the characteristic breathing mode of the triazine units.[29, 30] Further, Brunauer-Emmett-Teller (BET) surface area, adsorption and the pore size distribution were analyzed. Nitrogen adsorption and desorption isotherms of C_3N_4 is shown in Figure 1B. The result displays that the isotherm is a Type IV isotherm with a hysteresis loop, which is characteristic curve of mesoporous structures.[31, 32] The inset in Figure 1B displays the pore size distribution of C_3N_4 from the desorption branch using the BJH model, which mainly distribute at about 34 nm, and have a broad peak at 10-70 nm. The BET specific surface area of C_3N_4 is measured to be 103.4 m^2 g^{-1}. The morphology of C_3N_4 and C_3N_4-TYR is further observed on AFM, and the images are shown in Figure 1C and 1D respectively. In Figure 1D, the Elliptically-shaped features with sizes of about 10 nm, which is consistent well with the shape and size of TYR.[33, 34] The SEM image of C_3N_4-TYR (shown in Figure S1B) also shows the round-shaped or elliptically shaped of C_3N_4-TYR, further implying that enzyme (TYR) has been successfully encapsulated to the C_3N_4.

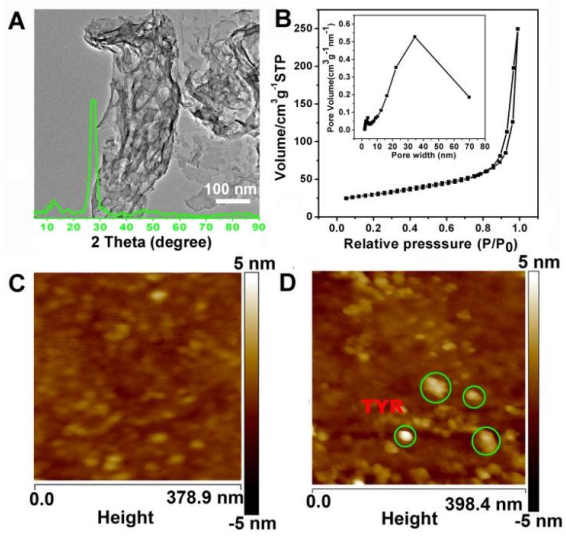

Figure 1. (A) Transmission electron microscopy (TEM) image, X-ray diffraction (XRD) pattern (shown as the green overlay at the bottom portion of the panel) of C_3N_4. (B) Nitrogen adsorption-desorption isotherms for C_3N_4 from 0 to 1 bar at 77 K, inset is the Corresponding pore size distribution of C_3N_4. (C) Atomic force microscopy (AFM) images of C_3N_4 and (D) AFM images of C_3N_4-TYR (Green circle is TYR).

To study their stability, C_3N_4-TYR was washed with phosphate buffer thoroughly. After washing, the supernatant displays no obvious enzyme catalytic activity on the DOPA (TYR-catalyzed oxidation of DOPA, see Figure 2A), whereas the high enzyme catalytic activity in C_3N_4-TYR is well maintained. Figure 2B shows absorption spectra of DOPA after washing and storage for 25, 31, 73, 83, 130, 142 and 202 h. It can be seen that it has no distinct change even after storage for 202 h, which suggests that C_3N_4 offers a good way to encapsulate TYR so as to keep the enzyme activity for a long time. To further confirm the increased enzyme activity in the C_3N_4 is due to the large surface area and the porosity of C_3N_4, a control experiment is carried out, g-C_3N_4 with small surface area of 7 m^2 g^{-1} (prepared by directly heating the melamine, see Figure 2C) is used to fabricate the C_3N_4-TYR hybrid instead of the porous C_3N_4. It is found that nonporous-C_3N_4-TYR hybrid also

washing shows no obvious enzyme activity on the DOPA (shown in Figure 2D). Therefore, it can be concluded that C_3N_4 with the large surface area and the porosity could provide an excellent matrix so that the enzyme activity can be well maintained.

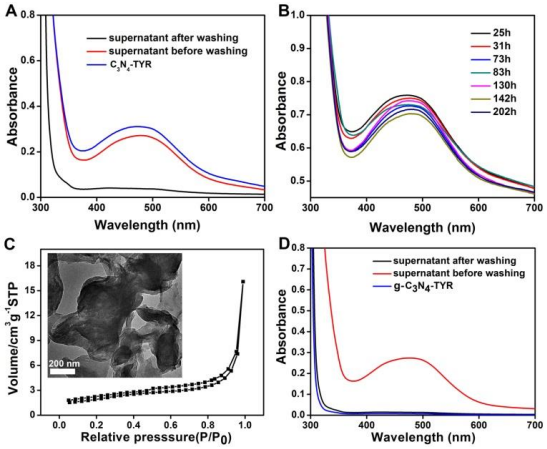

Figure 2 (A) Absorption spectra of dopamine after incubation with supernatant before and after washing the C_3N_4-TYR, C_3N_4-TYR just after washing (35 ℃, pH = 6.8). (B) Absorption spectra of dopamine after incubation with C_3N_4-TYR after washing and storage for 25, 31, 73, 83, 130, 142 and 202 h (35 ℃, pH = 6.8). (C) Nitrogen adsorption-desorption isotherms g-C_3N_4 from 0 to 1 bar at 77 K, inset is the TEM image of nonporous-C_3N_4. (D) Absorption spectra of dopamine after incubation with supernatant before and after washing the nonporous-C_3N_4-TYR (g-C_3N_4-TYR), nonporous-C_3N_4-TYR (g-C_3N_4-TYR) just after washing (35 ℃, pH = 6.8).

To further test the enzyme (TYR) catalytic activity of C_3N_4-TYR system, Michaelis-Menten analysis was performed. As shown in Figure 3A, the Michaelis–Menten behaviour could clearly be observed. Michaelis constant of C_3N_4-TYR (0.448 mmol L^{-1}) is about 1.4 times of that of the free enzyme (0.32 mmol L^{-1}). The maximum velocity of TYR in the C_3N_4 (0.25 mmol L^{-1} per min) is 92.5% of that of free TYR. It can be concluded that C_3N_4 provides a good matrix to encapsulate TYR without obvious structural changes and allows for relatively fast diffusion of substrate to the enzyme, which may be contributed to the large surface area and the porosity of C_3N_4.

As discussed above, the highly efficient fluorescent biosensor for DOPA detection should have stable emission, a suitable PL spectrum (match the absorption spectrum of dopaminechrome) and good proton adsorption ability. In the following study, we investigated the influence of irradiation time, temperature, ionic strength and pH on the fluorescence intensity of C_3N_4. As illustrated in Figure S3A, PL intensity of C_3N_4 is very stable with no obvious photobleaching loss after irradiation with the Hg-lamp (365 nm) for even 10 h. Figure S3B displays the effect of temperature on the normalized fluorescence intensity of C_3N_4 in the PB solution. It can be seen that when the temperature increases from 10 to 50 ℃, the PL intensity of C_3N_4 is almost the same, which indicates that the temperature does not affect the PL intensity of C_3N_4. In order to study the effect of ionic strength on the fluorescence intensity of C_3N_4, the NaCl solution with ionic strength from 0.2 to 2.0 mol·L^{-1} was added into solution at room temperature (Figure S3C). The results showed that the fluorescence intensity of C_3N_4 did not change even in aqueous solution with a high ionic strength (2 mol L^{-1} NaCl). The effect of pH on the fluorescence intensity of C_3N_4 was also studied. As can be seen from Figure S3D, no apparent change of fluorescence intensity of C_3N_4 is observed in the pH range of 2-12, indicating pH has a little effect on the fluorescence intensity of C_3N_4. From above discussion, it can be concluded that C_3N_4 can keep stable under Hg-lamp irradiation, high temperature, high ionic strength and strong acid or strong alkaline environment, which makes it a potential fluorescent probe candidate for the detection of bio-molecules. In the following studies, the proton adsorption experiment of C_3N_4 was also investigated. The adsorption experiments were conducted with a dialysis method (see experimental section for details). The amount of adsorbed HCl, Q (mg/g) was calculated by the following equation:

$$\mathbf{Q} = \frac{(\boldsymbol{C_0} - \boldsymbol{C_e})\boldsymbol{V}}{\boldsymbol{1000W}}$$

Where C_0 and C_e are the initial and equilibrium concentration (mg/L), respectively, V is the volume of HCl solution (mL) and W is the weight (g) of C_3N_4 adsorbent. The adsorption behaviour of C_3N_4 was conducted at the same condition, and the concentration and volume of C_3N_4 solution were same. Figure 3B shows the dependence of contact time on removal of H^+ by C_3N_4 from which the adsorption of H^+ was extraordinary rapid in the first 24 min, then gradually increased as the prolongation of contact time. After 30 min of adsorption, the amount of H^+ remains constant, which suggests that 6 min is the equilibrium time in this adsorption experiments. And the amount of adsorbed H^+ (based on the quality of HCl) is about 13.12 g/g. These results indicate that C_3N_4 possesses absorption capacity of H^+, which makes C_3N_4 more sensitive for the DOPA detection.

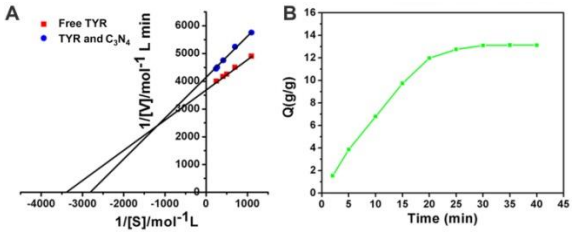

Figure 3 (A) Line weaver-Burk analysis of the enzymatic kinetics of free TYR and TYR in the C_3N_4. The concentrations of DOPA were 1.0, 1.5, 2.0, 2.5, 4.0, and. 5 mmol L^{-1}. Phosphate buffer (0.05 mol L^{-1}, pH = 6.8); incubation time 2 min. (B) Dependence of contact time on removal of H^+ by the C_3N_4.

As shown in Figure 4A and 4B, they displays UV/Vis absorption spectrum of dopaminequinone (DOPA was converted to dopaminechrome by a rapid spontaneous auto-oxidation in present of TYR, see Figure S4) and the PL spectrum of C_3N_4 from 325 to 750 nm when excitated at 390 nm. It can be seen that dopaminechrome gives rise to strong absorption at λ_{max} = 470 nm, and C_3N_4 has a strong emission at about 450 nm. The absorption spectrum of dopaminechrome has heavy overlap with the fluorescence spectrum of C_3N_4. Therefore,

PL of C_3N_4 should be significantly quenched by the dopaminechrome originated from the catalyzed product of the DOPA. To investigate the quenched fluorescence signal, the fluorescence spectra of C_3N_4, C_3N_4-TYR, C_3N_4-DOPA and C_3N_4-TYR-DOPA were recorded. As can be seen from Figure 4C, the spectra of C_3N_4, C_3N_4-TYR, C_3N_4-DOPA is almost the same. However, the fluorescence intensity of C_3N_4-TYR-DOPA is quenched significantly. Therefore, it can be concluded that the quenched fluorescence intensity of C_3N_4 is resulted from the dopaminechrome. All above results (porous structures, good photostability, strong proton H^+ adsorption ability, and the heavy overlap between the emission spectrum of C_3N_4 and the absorption spectrum of dopaminechrome) suggests that the C_3N_4-TYR could be used as a fluorescent probe for the high sensitive detection of DOPA. In the following studies, the factors like temperature, pH values and incubation time were optimized. As shown in Figure 4D, the I_0/I reaches maximum when the temperature is 35 ℃. Figure 4E displays the effects of pH on the fluorescence intensity of the reaction system. The results reveal that the fluorescence intensity of DOPA detection system (pH = 6.8) is most noticeably quenched in the same DOPA detection system. The curve in Figure 4F indicates that maximal quenched signal is achieved with 40 min of incubation and then sustains a stable value. Hence, to ensure complete fluorescence recovery and obtain stable signal, fluorescence intensity was recorded after the system had reacted for 40 min. Therefore, all further experiments were performed at 35 ℃, pH = 6.8 and an incubation time of 40 min.

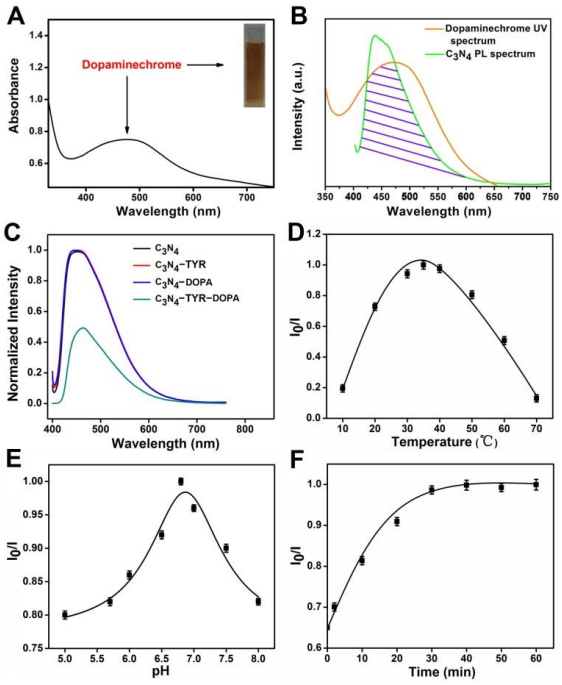

Figure 4 (A) UV/Vis absorption spectrum of dopaminechrome, inset: photograph of dopaminechrome under UV (365 nm, center) light. (B) UV/Vis absorption spectrum of dopaminechrome (orange trace) and the PL spectrum of C_3N_4 (green trace). (C) Fluorescence spectra of C_3N_4, C_3N_4-TYR, C_3N_4-DOPA, C_3N_4-TYR-DOPA (35 ℃, pH = 6.8, the concentrations of dopamine and TYR: 3.12×10^{-4} mol·L^{-1} and 0.1 mg mL^{-1}). Effects of temperature (D), pH values (E) and incubation time (F) on the fluorescence intensity of C_3N_4-TYR-DOPA detection system.

Under the optimal conditions, the sensing of C_3N_4-TYR to DOPA was conducted. As shown in Figure 5A and 5B, the florescence intensity of C_3N_4-TYR is markedly quenched in the presence of DOPA. The ratio I_0/I (I and I_0 are florescence intensity of C_3N_4-TYR in the presence and absence of DOPA, respectively) is proportional to the DOPA concentration with the linear regression equation being $I_0/I=1.10+2979.19C_{DOPA}$ (R^2 = 0.995). The detection limit of DOPA is 3×10^{-8} mol·L^{-1}, the detection range is from 3×10^{-8} to 1×10^{-3} mol·L^{-1}. The detection limit is lower than ever reported methods [35] and the detection range is comparable to some recently reported methods (shown in Table S1), [10, 35-38] which indicates that C_3N_4-TYR has a promising application for the detection of DOPA.

To evaluate the selectivity of the proposed method, we studied the fluorescence response of C_3N_4-TYR to DOPA in the presence of different potential interfering substances. The potential interfering substances include common DOPA analogues, amino acids and common ions. The results are shown in Figure 5C. Several DOPA analogues has little effect on DOPA detection even at concentrations 30 times higher than that of DOPA, indicating the high specificity of the proposed biosensors. Amino acids and common ions also exhibites little influence on the detection of DOPA. These results suggest that C_3N_4-TYR can apply as reliable sensor for the high selective detection of DOPA.

In order to investigate the accuracy of the developed detection system for DOPA, the detection of DOPA by the HPLC was performed. The DOPA concentration in urine samples of healthy subjects is between 100 and 400 mg/24 h.[39] Notably, this detection method based on C_3N_4-TYR could be directly used in real samples based on its high sensitivity and selectivity. The human urine samples were provided by the Peking Union Medical College Hospital. All measurements were performed in PB, pH = 6.8, incubated at 35 ℃ for 40 min. Samples 1~6 are the six different human urine samples with different DOPA concentrations. Meanwhile, the same six human urine samples were also detected by the clinical detection method (HPLC) and the proposed method under the same conditions. From Figure 5D, we can see that the results obtained using the proposed method coincides well with those obtained using HPLC, which indicates that the proposed method can be applied to the detection of DOPA in real samples with a high accuracy.

To evaluate the stability of the C_3N_4-TYR hybrids fluorescent probes, a series of stability experiments were carried out. Figure S5A shows the change of I_0/I when the probes were stored at 4 ℃ for 100 days. It can be seen that the I_0/I is almost the same during the 100 days at the temperature of 4 ℃. As shown in the Figure S5B, the I_0/I is little changed when the fluorescent probes are stored at room temperature for 20 days. These results reveal that the C_3N_4-TYR hybrids fluorescent probes are high stable at the room temperature or low temperature. Based on all of the above experiments and analyses, it can be concluded that, compared with other

methods, the proposed method not only has excellent repeatability, but also has a wider linear range and presents high accuracy. And it could be successfully applied in detecting DOPA in urine samples. Therefore, more novel biosensors based on the assembly of C_3N_4 with other enzymes could be expected for the high sensitive detection of other bio-molecules and medicament.

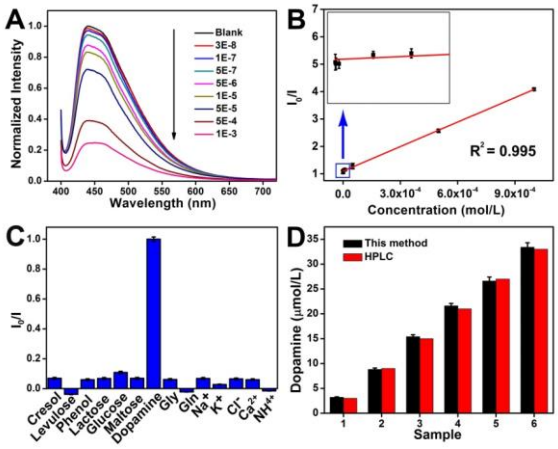

Figure 5 (A) DOPA sensing using C_3N_4-TYR (35 ℃, pH=6.8). (B) Relationship between I_0/I and DOPA concentration with DOPA concentration of 1×10^{-3}, 5×10^{-4}, 5×10^{-5}, 1×10^{-5}, 5×10^{-6}, 5×10^{-7}, 1×10^{-7} and 3×10^{-8} mol·L^{-1}.(the inset is the enlarged graph from 0 to 1.5×10^{-5} mol·L^{-1}) (C) Effects of potential interfering substances (35 ℃, pH = 6.8). (D) Analytical results of DOPA using the proposed method and using HPLC. The concentrations of DOPA are 3, 9, 16, 21, 27 and 33 μmol·L^{-1}, respectively. All measurements were performed in PB, pH = 6.8. The incubation time is 40 min, at 35 ℃.

Compared with the detection in liquid phase, it is convenient and fast to do the detection on solid substrate. However, few works have been done on it. To investigate the response of the enzyme-encapsulating C_3N_4 to DOPA on solid substrate, the enzyme-encapsulating C_3N_4 sensing arrays on glass slide were performed (Figure 6A). Figure 6A reveals the response of C_3N_4-TYR to DOPA of different concentrations under room light and UV light (365 nm excitation). It is found that DOPA shows obvious quenching to C_3N_4-TYR with DOPA concentrations varying from 1×10^{-3} to 2×10^{-7} mol·L^{-1}, which indicates that TYR activity in C_3N_4 is well maintained, and C_3N_4-TYR sustains its response to DOPA on the glass slide. Furthermore, the response can last for eight weeks without distinct color change. In the following studies, the test papers through the simple chemical method were designed and prepared, which could rapidly and exactly confirm the DOPA concentration range. As shown in Figure 6B, obvious color changes of the C_3N_4-TYR based test papers containing DOPA with concentration range from 2×10^{-2} to 5.12×10^{-8} mol·L^{-1} can be observed under room light and UV light (365 nm, excitation). Clearly, there is distinct fluorescence intensity on the C_3N_4-TYR modified paper, which was not observed before the modification. Therefore, the immobilized C_3N_4-TYR on the test paper can retain their fluorescence sensing towards DOPA without the addition of external reagents. Moreover, the sensing can maintain 3 months without obvious change. It can be concluded that C_3N_4-TYR based test paper provides a practical method to detect DOPA with high sensitivity and stability. To further study the response of C_3N_4-TYR to DOPA on the test paper, the fluorescence intensities of the reacti system with different DOPA concentrations were recorded From Figure 6C and 6D, we can see that the fluorescenc intensity of C_3N_4-TYR is obviously quenched in the presence of DOPA on the test paper. Furthermore, good linear correlation are obtained in the concentration range from 1.6×10^{-4} to 2.56×10^{-7} mol·L^{-1} for the detection of DOPA on the test pape (R^2 = 0.995). The detection limit is achieved to 2.56×10^{-7} mol·L^{-1}. Based on above results, we can conclude that C_3N_4-TY based test paper can serve as high sensitive and reliable sensor for the detection of DOPA.

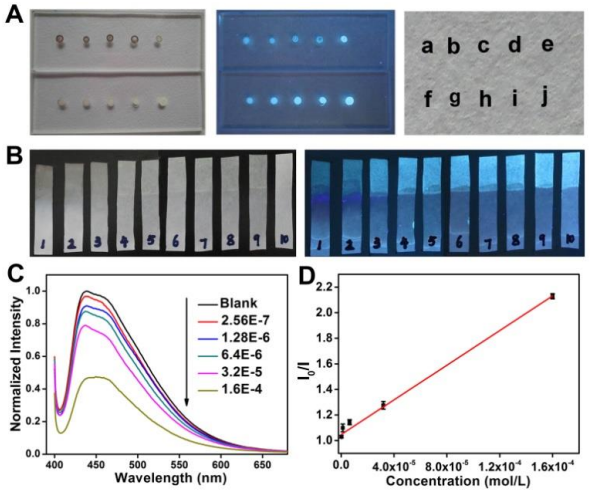

Figure 6 (A) Photos of the response of C_3N_4-TYR to DOPA with concentration of 1×10^{-3}, 5×10^{-4}, 2×10^{-4}, 5×10^{-5}, 2×10^{-5}, 5×10^{-6}, 2×10^{-6}, 5×10^{-7}, 2×10^{-7} and 0 mol·L^{-1}, (spots a respectively) under visible light and 365 nm UV light excitation (35 ℃, pH = 6.8). (B) Photos of C_3N_4-TYR impregnated fluorescent test paper sensing DOPA wi concentrations of 2×10^{-2}, 4×10^{-3}, 8×10^{-4}, 1.6×10^{-4}, 3.2×10^{-5}, 6.4×10^{-6}, 1.28×10^{-6}, 2.56×10^{-7}, 5.12×10^{-8} and 0 mol·L^{-1} (spots 1-10, respectively) under visible light and UV light (36 nm excitation), (35 ℃, pH = 6.8). (C) DOPA sensing of C_3N_4-TYR on the test paper. (Relationship between I_0/I and DOPA concentration with DOPA concentration of 1.6×10^{-4}, 3.2×10^{-5}, 6.4×10^{-6}, 1.28×10^{-6} and 2.56×10^{-7} mol·L^{-1} on the test paper.

Table 1. Determination of DOPA in simulate human urine sample using HPLC (clinical detection) and test paper

Sample	Real concentration (μM)	HPLC (Clinical) (μM)	Test paper detection (μM)	Relative error (%)	
				RE_1	RE_2
1	32	30±3	30±4	-6.25	-0.337
2	6.4	6.2±0.3	6.1±1	-4.69	-2.16
3	0.256	0.24±0.005	0.23±0.01	-10.16	-4.21

RE_1 = Test paper detection vs. Real concentration; RE_2 = Test paper detection vs. HPLC clinical detection.

In addition, to verify the efficiency of the C_3N_4-TYR base test paper, we also applied the standard HPLC method[37] to detect dopamine in simulate human urine sample. Table shows the date obtained in the analysis of simulate human urine sample using the HPLC method and the C_3N_4-TYR based test paper. It can be seen that the contents of DO

determined using the test paper are consistent with those using HPLC, which exhibits a little relative error. Therefore, it can be concluded that the proposed method is reliable for the determination of DOPA in simulate human urine sample. Meanwhile, it can be expected that the test paper will provide rapid and exact detection for other pharmaceutical and/or biological samples, if the TYR in the C_3N_4 is changed by the other kinds of enzymes.

Conclusion

In summary, a novel detection system containing TYR and C_3N_4 for the sensitive detection of DOPA was designed and fabricated. The fluorescence intensity of the C_3N_4-TYR was significantly quenched as the concentration of DOPA increased, in which a good linear relationship was obtained in the concentration range from 3×10^{-8} to 1×10^{-3} mol·L^{-1} with the correlation coefficient of 0.995. Moreover, the easy–to-prepare test paper for convenient and selective detecting DOPA was achieved by using C_3N_4-TYR sensing arrays. The results reveal that the proposed method coincided well with those obtained using HPLC, which indicates that the proposed method can be applied to the detection of DOPA in real clinical samples. The present detection system will provide a new approach to design multifunctional nano-sensors as a new method for the detection of bio-molecules.

Acknowledgements

This work is supported by Collaborative Innovation Center of Suzhou Nano Science and Technology, the National Basic Research Program of China (973 Program) (2012CB825803, 2013CB932702), the National Natural Science Foundation of China (51422207, 51132006, 21471106), the Specialized Research Fund for the Doctoral Program of Higher Education (20123201110018), a Suzhou Planning Project of Science and Technology (ZXG2012028), and a project funded by the Priority Academic Program Development of Jiangsu Higher Education Institutions (PAPD).

Notes and references

1 B. E. Kumara Swamy and B. Jill Venton, *Analyst,* 2007, **132**, 876–884.
2 A. Zhang, J. L. Neumeyer and R. J. Baldessarini, *Chem. Rev*., 2007, **107**, 274-302.
3 J. A. Gingrich and M. G. Caron, *Annu. Rev. Neurosci*., 1993, **16**, 299-321.
4 R. D. O'Neill, *Analyst,* 1994, **119**, 767-779.
5 D. P. Nikolelis, D. A. Drivelos, M. G. Simantiraki and S. Koinis, *Anal. Chem.,* 2004, **76**, 2174-2180.
6 T. M. Dawson and V. L. Dawson, *Science,* 2003, **302**, 819-822.
7 V. Carrera, E. Sabater E. Vilanova and M. A. Sogorb, *J. Chromatogr., B: Anal. Technol. Biomed. Life Sci.,* 2007, **847**, 88–94.
8 H. Y. Lee, J. J. Lee, J. Park and S. B. Park, *Chem. Eur. J.,* 2011, **17**, 143-150.
9 Y. Q. Wang and L. X. Chen, *Biol. Med*., 2011, **7**, 385-402.
10 J. P. Yuan, D. Wen, N. Gaponik and A. Eychmüller, *Angew. Chem. Int. Ed*., 2013, **52**, 976-979.
11 M. M. Ward Muscatello, L. E. Stunja and S. A. Asher, *Anal. Chem*., 2009, **81**, 4978-4986.
12 L. C. Chen, D. J. Huang, S. Y. Ren, T. Q. Dong, Y. W. Chi and G. N. Chen, *Nanoscale,* 2013, **5**, 225-230.
13 S. W. Cao and J. G. Yu, *J. Phys. Chem. Lett*., 2014, **5**, 2101-2107.
14 M. Sadhukhan and S. Barman, *J. Mater. Chem. A*., 2013, **1**, 2752-2756.
15 J. Zhou, Y. Yang and C. Y. Zhang, *Chem. Commun*., 2013, **49**, 8605-8607.
16 X. D. Zhang, X. Xie, H. Wang, J. J. Zhang, B. C. Pan and Y. Xie, *J. Am. Chem. Soc.,* 2013, **135**, 18-21.
17 J. Q. Tian, Q. Liu, A. M. Asiri, A. O. Al-Youbi and X. P. Sun, *Anal. Chem.,* 2013, **85**, 5595-5599.
18 J. H. Liu, T. K. Zhang, Z. H. Wang, G. Dawson and W. Chen, *J. Mater. Chem.,* 2011, **21**. 14398–14401.
19 S. C. Yan, Z. S. Li and Z. G. Zou, *Langmuir,* 2009, **25**, 10397-10401.
20 G. Z. Liao, S. Chen, X. Quan, H. T. Yu and H. M. Zhao, *J. Mater. Chem.,* 2012, **22**, 2721-2726.
21 S. C. Lee, H. O. Lintang and L. Yuliati, *Chem-Asian J.,* 2012, **7**, 2139-2144.
22 X. Wang, K. Maeda, A. Thomas, K. Takanabe, G. Xin, J. M. Carlsson, K. Domen and M. A Antonietti, *Nat. Mater.,* 2009, **8**, 76-80.
23 L. Shi, L. Liang, J. Ma, F. X. Wang and J. M. Sun, *Dalton Trans*., 2014, **43**, 7236-7244.
24 Y. P. Li, J. Zhan, L. Y. Huang, H. Xu, H. M. Li, R. X. Zhang and S. Y. Wu, *RSC Adv.,* 2014, **4**, 11831–11839.
25 F. Dong, L. Wu, Y. Sun, M. Fu, Z. Wu and S. C. Lee, *J. Mater. Chem.,* 2011, **21**, 15171-15174.
26 J. X. Sun, Y. P. Yuan, L. G. Qiu, X. Jiang, A. J. Xie, Y. H. Shen and J. F. Zhu, *Dalton Trans.,* 2012, **41**, 6756-6763.
27 J. L. Zimmerman, R. Williams and V. N. Khabashesku, *Nano Letter.,* 2001, **1**, 731-734.
28 Y. J. Wang, X. J. Bai, C. S. Pan, J. He and Y. F. Zhu, *J. Mater. Chem*., 2012, **22**, 11568-11573.
29 Q. J. Xiang, J. G. Yu and M. Jaroniec, *J. Phys. Chem. C*., 2011, **115**, 7355-7363.
30 L. Ge, C. Han and J. Liu, *J. Mater. Chem.,* 2012, **22**, 11843-11850.
31 D. Feng, Y. Y. Lv, Z. X. Wu, Y. Q. Dou, L. Han, Z. K. Sun, Y. Y. Xia, G. F. Zheng and D. Y. Zhao, *J. Am. Chem. Soc.,* 2011, **133**, 15148-15156.
32 L. Zhou, J. Liu, X. Zhang, R. H. Liu, Y. Liu and Z. H. Kang, *Nanoscale,* 2014, **6**, 5831-5838.
33 Y. Matoba, T. Kumagai, A. Yamamoto, H. Yoshitsu and M. Sugiyama, *J. Biol. Chem*., 2006, **281**, 8981-8990.
34 M. Sendovski, M. Kanteev, V. S. Ben-Yosef, N. Adir and A. Fishman, *J. Mol. Biol.,* 2011, **405**, 227-237.
35 H. C. Su, B. Sun, L. J. Chen, Z. N. Xu and S. Y. Ai, *Anal. Methods*, 2012, **4**, 3981-3986.
36 X. L. Wang, Y. F. Ma, X. M. Yao, J. Wang and M. Yin, *RSC Adv*., 2013, **3**, 24605-24611.
37 J. J. Feng, H. Guo, Y. F. Li, Y. H. Wang, W. Y. Chen and A. J. Wang, *ACS Appl. Mater. Interfaces*., 2013, **5**, 1226-1231.
38 A. Abbaspour, H. Varizadeh and A. Khajehzadeh, *Anal. Methods*., 2011, **3**, 1405-1409.
39 T. J. Panholzer, J. Beyer and K. Lichtwald, *Clin. Chem*., 1999, **45**, 262-268.